Giant reversibility of magnetoresponsive properties in all-*d*-metal Ni-Co-Mn(Cu)-Ti Heusler alloys: Role of phase-fraction-assisted magnetostructural transition

Saheli Samanta [1,*,†] Sudipta Chatterjee [1,†] Jayee Sinha [2] and Kalyan Mandal [1]

[1] *Department of Condensed Matter and Materials Physics, S. N. Bose National Centre for Basic Sciences, JD Block, Sector III, Salt Lake, Kolkata 700106, India*

[2] *Department of Electronic Science, University of Calcutta, 92 Acharya Prafulla Chandra Road, Kolkata 700084, India*

(Received 10 April 2023; accepted 8 August 2023; published 18 August 2023)

Recently emerged all-*d*-metal Ni(Co)-Mn-Ti Heusler systems often exhibit multifunctional properties which are accompanied by magnetic-field-induced inverse martensitic transformation (IMT). Hence, the study of the transitional dynamics of IMT on the corresponding intriguing physical properties is of great importance. In this paper, we report the critical significance of field-induced austenite phase fraction (Δf_{IA}) in achieving giant reversible magnetoresponsive properties of the optimizing Cu doped in $Ni_{35}Co_{15}Mn_{34.5-x}Cu_xTi_{15.5}$ (x = 1, 2, and 3) all-*d*-metal Heusler systems. We show that the Cu substitution in the Mn site pulls the magnetic transition towards structural transitions and therefore the distance between them decreases. The evolution of Δf_{IA} has been investigated using the Clausius Clapeyron equation and the Landauer equation under field cycling by variation of magnetization and resistivity as a function of temperature and field for $x = 2$ sample. A giant reversible magnetic entropy change (ΔS_M) of ~ 22.8 J kg^{-1} K^{-1} at 257 K as well as a giant effective refrigerant capacity (RC_{eff}) of ~ 610 J kg^{-1} in a field change of 7 T (~ 9 J kg^{-1} K^{-1} at 269 K and $RC_{\mathrm{eff}} \sim 144$ J kg^{-1} under 2 T) is obtained, correlating with the good geometrical compatibility between two phases (λ_2 closer to 1) and the high sensitivity of phase transition temperature to the magnetic field (~ 4.3 K/T). Moreover, a remarkably giant reversible magnetoresistance (MR) of $\sim 40\%$ over 42% of the total MR in a field change of 7 T is observed, when Δf_{IA} is fully induced. The observed magnitude of reversible magnetocaloric effect and MR is the highest reported value so far in the all-*d*-metal Heusler family. Our findings corroborate the generality of using the Δf_{IA} to enhance reversible magnetoresponsive properties in conventional all-*d*-metal Heusler system. These giant magnetoresponsive characteristics over a wide temperature window may therefore lead to the all-*d*-metal Heusler system as a suitable state-of-the-art caloric material for solid-state-based technological applications.

DOI: 10.1103/PhysRevMaterials.7.084406

I. INTRODUCTION

The coupling between lattice and magnetic degrees of freedom that undergoes a magnetostructural transition (MST) in solid magnetic materials is of great importance from both the fundamental as well as the technological landscape. The systems having such striking behavior govern enormous exotic physical properties such as magnetocaloric effect (MCE) [1–3], giant magnetoresistance (MR) [4–6], giant magnetostrain [7–9], and shape memory effect [10]. These intriguing physical properties often involve simultaneous and combined discontinuities in the electronics, magnetic, and crystallographic instabilities [11]. In a word, they are particularly profound across the first-order field-induced inverse martensitic transition (IMT), which eventually leads to modulating dynamics of these physical properties of those systems through various types of external stimuli such as stress, magnetic field, temperature, and pressure. These systems, in particular, conduct a phenomenal area for material physics since their physical properties are highly responsive to relatively low external stimuli. Concisely, understanding the effect of magnetic fields on this coupling is crucial for magnetic systems. In addition to the basic MCE properties, the practical application requires other parameters, such as reversibility, cyclical stability, nontoxicity, and inexpensiveness, for their extensive utilization. MCE materials such as Gd-based [12,13], La(Fe, Si)$_{13}$-based [14], *M*Mn*X*-based (*M*= Co, Ni, *X*= Ge, Si) hexagonal systems [15–17] and Ni-Mn-based metamagnetic Heusler alloys [3,18] have shown large MCE performances around room temperature. However, the broad hysteresis often associated with the transition, irreversibility, and fragility are key drawbacks for their applications.

Recently, instead of $p-d$ hybridization, $d-d$ hybridization-based $Ni_2Mn_{1-x}Ti_{1+x}$ all-*d*-metal Heusler alloys are very emerging systems in which the MST arises from a high temperature, high symmetry cubic B2-type austenite (spatial group $Pm\bar{3}m$) to a low temperature, low-symmetry monoclinic (spatial group $P2/m$) or tetragonal (spatial group $I4/mmm$) martensite phase without substantial magnetization change (ΔM) [19]. Ni_2MnTi crystallizes in a cubic B2 austenite structure, consisting of four interconnected face-centered cubic sublattices, with $T_N \sim 120$ K [19]. The antiferromagnetic (AFM) ground state may be originated due to indirect Ruderman-Kittel-Kayusa-Yosidda (RKKY)

*saheliphys249@gmail.com

†These authors contributed equally to this work.

between neighboring Mn atoms mediated through conduction electrons [20]. Moreover, RKKY interaction may be promoted by the hybridization of d-Mn and d-Ti electronic states [21]. This $d-d$ hybridization results in the enhancement of ductility, especially in the vicinity of MST where the intrinsic brittleness of Ni-Mn-based Heusler alloys could lead to a crack inside the material during phase transformation under a high external field [22–24]. However, by inducing an obvious ΔM through element substitutions and following the above-mentioned benefit, the most remarkable physical properties across the IMT such as large inverse and conventional MCE [25–27], giant exchange bias [28], colossal elastocaloric effect [29], giant barrocaloric effect [30], large magnetostrain [31], and large MR [32–34] are observed. These exciting features not only emphasize the potential interest in all-d-metal Heusler alloys for future solid-state refrigeration but also provide an ideal path for a deeper understanding of the compelling physics subjected to these properties in this system.

A magnetic field can induce an IMT during heating where martensitic fractions transform into austenite phases. Although this IMT is highly irreversible in all-d-metal Heusler alloys, i.e., one cannot completely recover the transformed phase fraction by removing the field [33,34]. Recently, using the geometrical compatibility condition, we reported that Ni(Co)-Mn-Ti all-d-metal Heusler alloy forms an exactly compatible and stress-free phase boundary which drastically lowers its hysteresis (ΔT_{hys}) and sharpens the transformation width (ΔT_{int}) [32]. Cosubstitution in the Ni site enhances the saturation magnetization in the austenite phase, which leads to a large sensitivity. Thus, a complete or partially reversible IMT is formed and, sequentially, the large reversibility of magnetoresponsive properties has been observed. The same scenario holds for the interstitial B doping in $Ni_{36.5}Co_{13.5}Mn_{35}Ti_{15}B_{0.4}$, where the first-principles calculations predict nearly 40% enhancement of saturation magnetization, however, experimentally obtained reversible MCE has remained 22% smaller than the total one for 5 T magnetic field, presumably due to small sensitivity originating from partial field-induced IMT [35]. Hereby, the tuning of IMT and corresponding features can promote a key relevance for a sizable optimization of the above-mentioned multifunctional properties.

In this paper, we establish a comprehensive experimental picture of field-induced inverse martensitic structural evolution in terms of the Clausius Clapeyron equation (CCE) and Landauer equation to enhance the reversible properties in bulk $Ni_{35}Co_{15}Mn_{34.5-x}Cu_xTi_{15.5}$ ($x = 1$, 2, and 3) all-d-metal Heusler alloys under an applied magnetic field of 5 T and 7 T. Our previous work in Ni(Co)-Mn-Ti showed that Co substitution in Ni site enhances the saturation magnetization in the austenite phase, which leads to a large sensitivity [32]. So in the present work, $Ni_{35}Co_{15}Mn_{34.5}Ti_{15.5}$ is considered the parent system. Through systematically tuning the Cu substitution in the Mn site, a giant reversible $\Delta S_M \sim 22.8\,\text{J kg}^{-1}\,\text{K}^{-1}$, $\text{RC}_{\text{eff}} \sim 374\,\text{J kg}^{-1}$ and a giant reversible MR $\sim 40\%$ around room temperature is found for the optimized $x = 2$ sample. The observed giant reversible MCE over a wide temperature range and the giant reversible MR concurrently in the present system are the highest values achieved in this all-d-metal Heusler family. Our study also demonstrates how phase volume fraction between austenite and martensite phases in the vicinity of IMT can maximize the reversible magnetoresponsive properties in these systems.

II. EXPERIMENTAL DETAILS

$Ni_{35}Co_{15}Mn_{34.5-x}Cu_xTi_{15.5}$ ($x = 1$, 2, and 3) polycrystalline samples were prepared by arc melting technique under a 4 N purity argon atmosphere using high-purity constituent elements from Sigma Aldrich. To ensure compositional homogenization, the samples were re-melted five to six times on each side. The melted ingots were wrapped with tantalum foil and sealed in an evacuated quartz tube. The samples were annealed at 1323 K for four days and quenched in ice water. The actual compositions of the studied samples were verified by energy dispersive x-ray. The details are in the Supplemental Material [36]. The room temperature x-ray diffraction (XRD) patterns of all the samples and temperature-dependent XRD for $x = 2$ sample in powder form were performed using SmartLab9kW, Rigaku with Cu-K_α radiation. The details of the XRD data of all three samples are given in Secs. S1 and S2 of the Supplemental Material [36]. Magnetic measurements were done in a vibrating sample magnetometer (VSM) using a physical property measurement system (PPMS, Quantum Design). Each $M(T)$ and $M(\mu_0 H)$ curve were taken at a ramp rate of 2 K/min and 20 Oe/s, respectively. Differential scanning calorimetry (DSC, TA Instrument, Q2000) was performed to measure the heat flow curve of the sample with a constant heating/cooling rate of 10 K/min. The obtained results of all the samples are manifested in Sec. S3 of the Supplemental Material [36]. The specific heat capacity (C_P) was measured by a modulated-DSC technique to obtain adiabatic temperature change (ΔT_{ad}). Magnetotransport properties were performed in the PPMS (Quantum Design, USA) using the electrical-transport option. For the MR measurements, the electrical contacts were made in the standard four-probe configuration using conducting silver epoxy and copper wires.

III. RESULTS AND DISCUSSIONS

A. Modulating magnetostructural transformation behavior

Figures 1(a)–1(c) display the temperature-dependent magnetization $M(T)$ data for all the samples measured in a magnetic field of 0.05 T, 5 T, and 7 T during field-cooled (FC) and zero-field-cooled (ZFC) protocols. All samples undergo a first-order MST at martensite transition temperature (T_M) from FM austenite to weak magnetic martensite below the Curie temperature (T_C) on cooling and an IMT at austenite phase transition temperature (T_A) on heating. The characteristic transition temperatures of first-order MST, namely, austenite start (A_s), austenite finish (A_f), martensite start (M_s), martensite finish (M_f) are determined by the tangent method from the $M(T)$ and DSC curves, and ($T_M = (M_s + M_f)/2$), ($T_A = (A_s + A_f)/2$), thermal hysteresis ($\Delta T_{\text{hys}} = T_A - T_M$), and T_C of all the samples are tabulated in Table I.

It is found from Figs. 1(a)–1(c) that the Cu substitution in the Mn site shifts the first order-MST towards higher temperature and moves the T_C towards lower temperature. In addition, the hysteresis width is observed to increase from

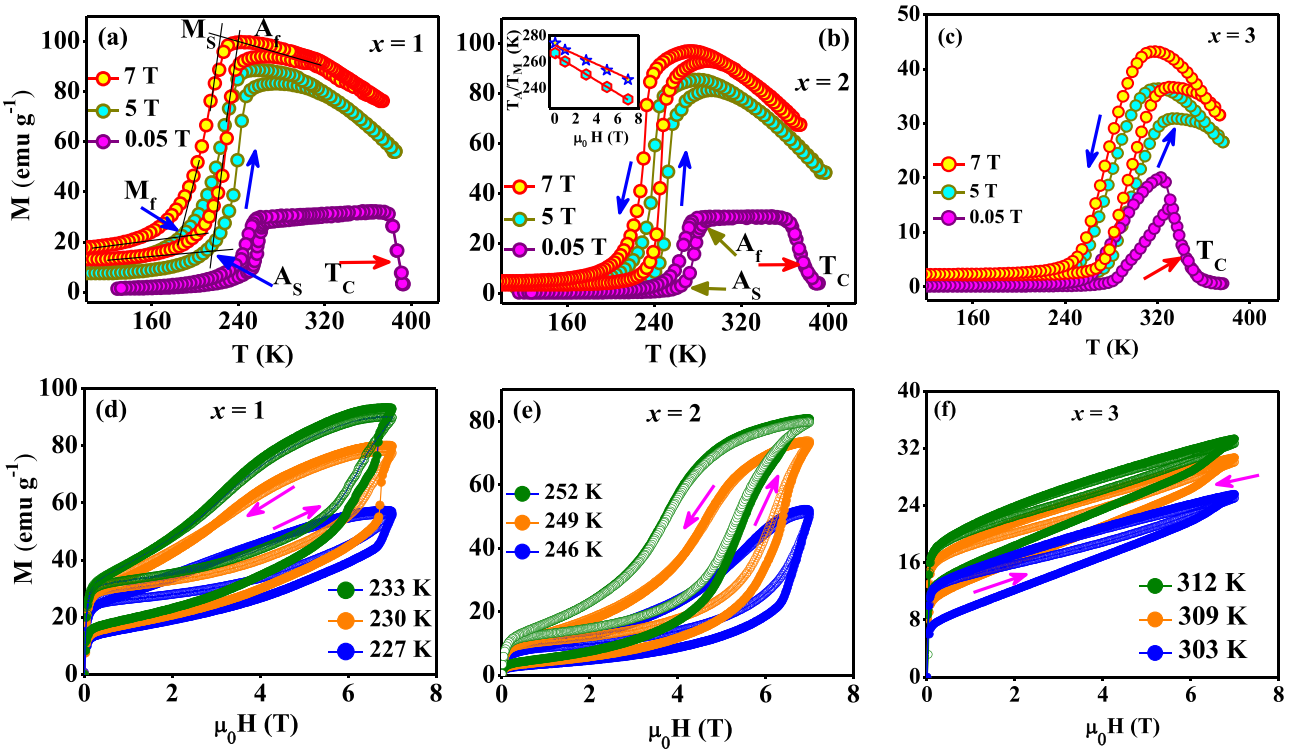

FIG. 1. Temperature-dependent ZFC and FC magnetization of (a) $x = 1$, (b) $x = 2$, and (c) x= 3 samples under 0.05, 5 T, and 7 T. Inset of Fig. 1(b) shows the shift of transformation temperatures and its linear fitting as a function of the magnetic field. Field-dependent magnetization across the inverse martensitic transition for (d) $x = 1$, (e) $x = 2$, and (f) $x = 3$ samples. Closed symbols refer to the first cycle $M(\mu_0 H)$ loop and open symbols indicate the second cycle taken after the first one during the heating protocol.

8.1 K to 15.1 K from the sample $x = 1$ to 3. Because Cu increases the metallic character of the Ni–Ti bond, i.e., the higher degree of *d-d* hybridization produces a stronger metallic bonding, sufficient energy is required to lead the MST and subsequently results in the increase of MST temperatures [37–39]. On the other hand, reducing Mn concentration weakens the Mn–Mn exchange interaction and consequently, overall magnetization and T_C decrease with Cu doping [39–42].

With increasing magnetic field, the T_M and T_A go towards lower temperature, in agreement with the magnetic field stabilizing the large magnetization cubic austenite phase. An increase of the magnetic field, for example, 0.05 T to 7 T, stabilizes the high-temperature FM austenite phase, causing a shift of the T_M by 4.4, 4.3, and 3.1 K/T, whereas the T_A changes by 4.1, 3.6, and 2.4 K/T for $x = 1$, 2, and 3 alloys, respectively. The sensitivity of transition temperatures to the magnetic field obtained from the linear fitting of T_M/T_A versus magnetic field is shown in the inset of Fig. 1(b) for the $x = 2$ sample. The data for the rest of the samples are given in Figs. S4(a) and S4(b) of the Supplemental Material [36], and all these data are gathered in Table I. This value is larger than the reported Cu-doped Heusler systems [37,39]. According to the CCE, the sensitivity of IMT ($dT_A/d\mu_0 H$) is directly connected to ΔM and transformation entropy change (ΔS_{tr}) [2]. Meanwhile, ΔS_{tr} decreases with increasing the distance of (T_C–T_A) because the spin alignment increases, leading to a larger $dT_A/d\mu_0 H$ (and thus reversible MCE) [42–44]. Our present result indicates a similar scenario, i.e., the increase of ΔS_{tr} with Cu substitution for the Mn site is attributed to the negative magnetic contribution to ΔS_{tr} which lowers the ΔM [45]. This has been analogously reported in other

TABLE I. Transition temperatures determined from both the $M(T)$ curves under 500 Oe and DSC data of all-*d*-metal $Ni_{35}Co_{15}Mn_{34.5-x}Cu_xTi_{15.5}$ Heusler alloys. Field sensitivity is also calculated for all the samples.

Alloys	Tools	M_s (K)	M_f (K)	A_s (K)	A_f (K)	T_M (K)	T_A (K)	ΔT_{hys} (K)	T_C (K)	$dT_A/d\mu_0 H$ (K/T)	$dT_M/d\mu_0 H$ (K/T)
$x = 1$	VSM	254.9	244.7	253.3	262.8	249.8	257.9	8.1	387.7	4.1	4.4
	DSC	251.6	245.9	253.8	260.1	248.8	256.9	8.2			
$x = 2$	VSM	273.9	258.3	268.6	280.5	266.2	274.6	8.5	376.4	3.6	4.3
	DSC	275.1	259.1	269	281.8	267.1	275.4	8.3			
$x = 3$	VSM	320.1	266.9	287.9	329.5	293.7	308.7	15.1	334.9	2.4	3.1
	DSC	316.8	272.2	291.9	326.7	294.5	309.3	14.8			

Ni-Mn(Cu)-Ga [38], and Ni-Mn(Cu)-Ga-Al Heusler systems [46]. Using the CCE, the sensitivity $dT_A/d\mu_0H$ is found to be ∼4.1, 3.6, 1.8 K/T for $x = 1$ to 3 samples, which is in good agreement with the above fitting value (where ΔM is ∼82, 89, 41 emu/g of the respective $x = 1$ to 3 samples for $\Delta\mu_0H = 7$ T).

It is reported that a complete reversible field-induced IMT and corresponding magnetoresponsive properties can occur in the temperature range between A_f at μ_0H and M_f at 0 T when $A_f(\mu_0H) < M_f$ (0 T) [47,48]. It is noteworthy to introduce that a partial reversible IMT happens within the temperature interval between A_S under μ_0H, and the M_S under 0 T. From Figs. 1(a) and 1(b), a large temperature window, respectively, from 224 K (A_S) and 241 K (A_S) under 7 T to 253 K(M_S) and 274 K (M_S) under 0 T is observed for $x = 1$ and 2 samples.

Though the $x = 1$ sample possesses large $dT_A/d\mu_0H$ and higher magnetization in the austenite phase compared to the other two alloys, it experiences a smaller ΔM due to its intrinsic magnetic properties in the martensitic phase, as observed from the $M(T)$ curve during cooling in Fig. 1(a). Furthermore, a broaderlike nature of $M(T)$ curve can lead to a reduction of the reversible properties of $x = 1$ sample. Elsewhere, a sharp IMT, moderate ΔS_{tr}, and large $dT_A/d\mu_0H$ are observed for the $x = 2$ sample. In addition, the complete field-induced IMT can be expected to occur between ∼246 K (A_f) at 7 T and ∼259 K (M_f) at 0 T with the condition $A_f < M_f$, which can result in large reversible magnetofunctional properties for the $x = 2$ sample.

Figures 1(d)–1(f) exhibit field-dependent magnetization $M(\mu_0H)$ curves during cyclically magnetic field sweeping record in the temperature range between A_S under $M(\mu_0H)$ and M_S under 0 T for all samples. For simplicity, we have shown $M(\mu_0H)$ curves in the vicinity of the IMT region under the applied magnetic field of 7 T. During the first field cycle, the sample is cooled down to 100 K to assure the fully martensitic phase from 330 K and then heated back to the selective temperatures where the $M(\mu_0H)$ data are taken [49]. In the second field cycle, the $M(\mu_0H)$ data are taken at the same temperature just after the first field sweeping. In the case of $x = 1$, the field-induced transition occurs at the field of 6.6 T at A_S (under 7 T), whereas for $x = 2$ it leads to a complete field-induced transition at the field of 6.2 T, and for $x = 3$ the transition is not complete. However, for the $x = 2$ sample, the $M(\mu_0H)$ curves of both cycles are more reproducible than the others, i.e., the $M(\mu_0H)$ curves lie close to the first one. In addition, across the T_A first field increase of 7 T, the magnetic field-induced transition starts around 4.5 T and finishes at a field of 5.8 T, while for the second cycle $M(\mu_0H)$ curve saturates at the same field. Magnetization does not increase uniformly yet exhibits steplike features. From the field decreasing mode of 7 T, both curves follow the same path. This steplike feature is associated with the fact that the field-induced austenite mostly transforms back to martensite, which can participate reversibly to transform back and forth between martensite and austenite during the second and all subsequent field cycling. Therefore, large reversible magnetofunctional properties could be expected in this specific $x = 2$ sample.

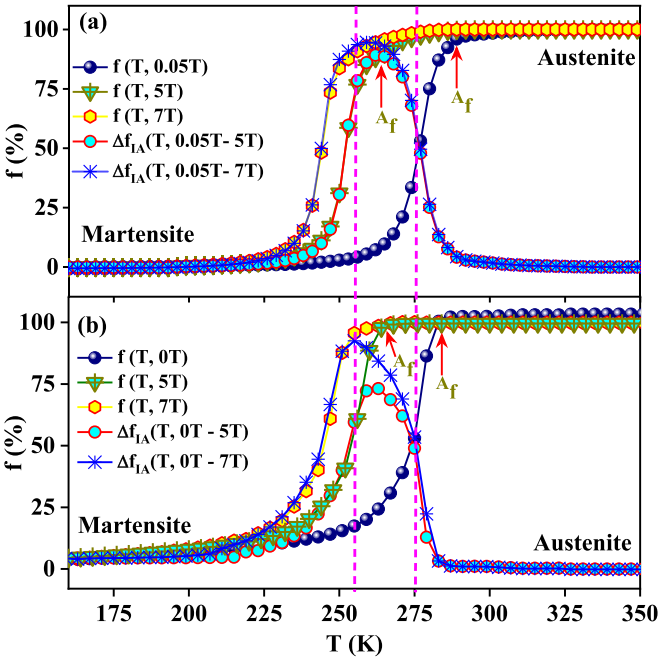

FIG. 2. (a) Austenite phase volume fraction $f(T)$ under 0.05, 5, and 7 T is determined from $M(T)$ curve during heating mode and induced austenite phase volume fraction $\Delta f_{IA}(T)$ represented by a cyan solid circle and blue star symbols for 5 T and 7 T field change, respectively. (b) The $f(T)$ under 0, 5, and 7 T from $\rho(T)$ curve and corresponding $\Delta f_{IA}(T)$ for 5 T and 7 T applied fields.

B. Evaluation of phase fraction from $M(T)$ and $\rho(T)$ curves

The reversibility of magnetofunctional properties of shape memory alloys is correlated to the magnitude of field-induced inverse martensitic phase transformation. So, it is crucial to yield the physical origin of such functionality for further improvement toward large-scale practical applications. We demonstrate the evolution of the different phase fraction in the vicinity of IMT in different applied fields. The temperature-dependent magnetization and electrical resistivity [$\rho(T)$] under different magnetic fields of $x = 2$ sample are measured. Corresponding evolution of the volume fraction of austenite using the $M(T)$ curve under 0.05 T, 5 T, and 7 T and $\rho(T)$ curve under 0 T, 5 T, and 7 T is depicted in Fig. 2. The austenite phase volume fraction, $f(T)$ triggered by a magnetic field change is evaluated on the basis of total magnetization originating from FM austenite phase and can be estimated from the $M(T)$ curve as [50]

$$f(T) = \frac{M(T) - M_{LT}(T)}{M_{HT}(T) - M_{LT}(T)} \quad (1)$$

where M_{LT}(T) and M_{HT}(T) represent the magnetization of the low-temperature martensitic phase and high-temperature austenite phase, respectively. Field-induced austenite phase fractions (Δf_{IA}) are determined from the heating $M(T)$ curve for the field change of 0.05 T to $M(\mu_0H)$. It is observed from Fig. 2(a) that in the vicinity of phase coexistence region ($A_S < T < A_f$), Δf_{IA} starts to increase with temperature and a maximum Δf_{IA} ∼90% at 262 K for 5 T and ∼96% at 255 K for 7 T is induced as a reversible part while the remaining 10% and 4% residual austenite phase, respectively, is unchanged,

which is a good agreement with the $M(\mu_0 H)$ curve of the above-mentioned section. This tiny residual phase is arrested by applying the magnetic field due to the little big transformation width of $x = 2$ sample. Note that a sharp transformation, smaller hysteresis, and larger sensitivity are necessary to erase this tiny residual phase. However, with further increase in temperature, the Δf_{IA} exhibits a rapid decrease and drops to zero above A_f as no martensitic phase is observed [48].

To get further insight into the phase transformation features, phase fractions from the $\rho(T)$ of Fig. 5(a) are calculated using the Landauer equation [51] for two coexisting phases in the following form:

$$\sigma(T) = \tfrac{1}{4}[(3f_A - 1)\sigma_A - (3f_M - 1)\sigma_M + [\{(3f_A - 1)\sigma_A + (3f_M - 1)\sigma_M\}^2 + 8\sigma_A\sigma_M]^{\frac{1}{2}}], \quad (2)$$

where σ_A and σ_M are the conductivity of pure austenite and martensite phases, respectively. ρ_A and ρ_M in the form of σ_A and σ_M can be roughly obtained through linear extrapolation of the $\rho(T)$ curve from the transition point. Further, it is known that the total phase fraction in the form of $f_M(T, H)$ and $f_A(T, H)$ at a particular temperature and field can be written as

$$f_M(T, H) + f_A(T, H) = 1. \quad (3)$$

One can solve Eq. (2) for a particular temperature and field using Eq. (3) and substituting the values of σ_A and σ_M. When the magnetic field is applied isothermally in the phase transition regime, a fraction of the martensite phase is transformed into the austenite phase, then we can write Δf_{IA} in the following form:

$$f_{\mathrm{IA}}(T, \Delta H) = f_M(T, 0) - f_M(T, H). \quad (4)$$

The calculated $f_A(T, H)$ under 0 T, 5 T, and 7 T, respectively, and their difference, Δf_{IA} curves, are illustrated in Fig. 2(b). It is observed that Δf_{IA} follows the same path of $f_M(T,0)$. In the region of A_S, Δf_{IA} start to grow 17% and 35%, and at the middle of the transition, Δf_{IA} reaches their maximum value of 76% at 261 K and 96% at 255 K for the field change of 5 T and 7 T, respectively. This can be attributed to the conversion of the entire metastable martensitic phase (76% for 5 T and 96% for 7 T) into the austenite, while the remaining 24% and 4% are the residual austenite phases. With further increasing temperature, due to the increase of instability of martensite, the field-induced Δf_{IA} decreases and above A_f, Δf_{IA} becomes zero [56]. It is noteworthy that the Δf_{IA} from both measurements under 5 T show slight differences. This difference likely occurs in a way that field-induced IMT shift in $\rho(T)$ ~ 16 K is smaller than that ~ 20 K in the $M(T)$ under 5 T. Thereby, a relatively smaller amount of metastable martensitic phase is transformed into the FM austenite phase in the $\rho(T)$ measurement. This analogous behavior has been previously observed in all-d-metal Heusler alloys, as well as various other Heusler systems where that disparity arising from $M(T)$ and $\rho(T)$ measurements has been noticed [19,34,57]. However, the obtained field-induced Δf_{IA} using Eq. (2) is well consistent with that estimated using the Landauer equation. Therefore, it could be feasible to simultaneously achieve more or less reversible MCE and MR across IMT for x= 2 in all-d-metal Heusler alloy.

C. Reversible magnetocaloric performances

To study the importance of phase fraction on MCE, we performed isofield $M(T)$ and isothermal magnetization $M(\mu_0 H)$ measurement protocols [58–60]. Isothermal $M(\mu_0 H)$ curves are record during cyclic magnetic field sweeping in the temperature range between 240 K to 264 K with an interval of 3 K, shown in Fig. 3(a). It is clearly shown that a metamagnetic characteristic in the $M(\mu_0 H)$ curves of both cycles, indicates a magnetic field-induced transition. Henceforth, the reversibility of isothermal magnetic entropy change (ΔS_M) is determined using different methods. CCE using the transformation fraction method is appropriate for the first-order MST, ΔS_M values are obtained during heating mode from the $M(T)$ curve for the different field changes [50],

$$\Delta S_M = \Delta f \cdot \Delta S_{\mathrm{tr}} = -\Delta f \cdot \Delta M \left(\frac{dT_A}{d\mu_0 H}\right)^{-1}, \quad (5)$$

where Δf is the change of phase fraction of austenite induced by the change of magnetic field that can be defined as Δf (T, $\mu_0 \Delta H$) = f (T, $\mu_0 H_f$) -f (T, $\mu_0 H_i$). $\mu_0 H_i$ and $\mu_0 H_f$ are the initial and final applied magnetic fields, respectively.

The maximum ΔS_M during heating and cooling for the field changes from H_i ~ 0.05 T to H_f ~ 5 T and for H_i ~ 0.05 T to H_f ~ 7 T is plotted in Fig. 3(b). The giant reversible value is 19.2 J kg^{-1} K^{-1} at 259 K and 22.8 J kg^{-1} K^{-1} at 257 K for a field change of $\mu_0 H = 5\,T$ and 7 T, respectively. The cyclic ΔS_M and corresponding reversible ΔS_M can be estimated by the overlapping region of the both heating and cooling branch which is shown in the green shaded area in Fig. 3(b). Further ΔS_M is also determined across T_A, using Maxwell relation [61],

$$\Delta S_M(T, \Delta H) = \mu_0 \int_0^H \left(\frac{\partial M(H, T)}{\partial T}\right)_H dH, \quad (6)$$

where, μ_0, M, H, and T are the permeability of free space, magnetization, applied magnetic field, and instantaneous temperature, respectively. Compared with the parent compound, the maximum value of ΔS_M ~ 20.16 J kg^{-1} K^{-1} at 257 K and 23.74 J kg^{-1} K^{-1} at 259 K is obtained for $x = 2$ under 5 T and 7 T, respectively, shown in Fig. 3(c), which is in good agreement with ΔS_{tr}, determined from the DSC curve as depicted in Fig. S3(a) of the Supplemental Material [36].

It is observed from Fig. 2 that a small fraction of residual austenite persists after the first field cycling and contributes a slightly negative roll in the reversible magnetoresponsive properties in our system. Therefore, the transformation fraction method (CCTF) based on isothermal $M(\mu_0 H)$ curves is a feasible procedure to determine reversible and reproducible MCE properties [48]. The field-induced phase fraction of austenite is determined from the $M(\mu_0 H)$ curve of both cycles at the respective temperatures using the following equation:

$$f(T) = \frac{M(H) - M_{\mathrm{LT}}(H)}{M_{\mathrm{HT}}(H) - M_{\mathrm{LT}}(H)}, \quad (7)$$

where $M_{LT}(H)$ and $M_{HT}(H)$ represent the magnetization of the martensite and austenite phase which can be deduced by extrapolating $M(\mu_0 H)$ curve at 200 K and 300 K of the pure martensite and austenite phase, respectively [62] [shown in green dotted lines in Fig. 3(a)]. Figures 3(c) and

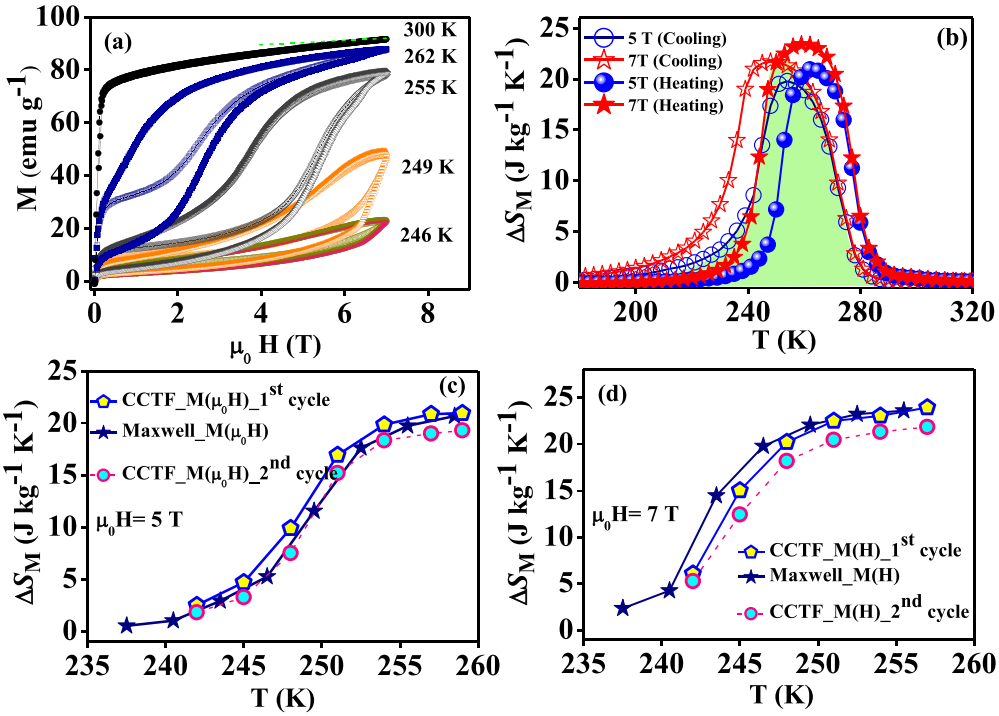

FIG. 3. (a) Isothermal M-$\mu_0 H$ hysteresis measured during the first (solid circle) and second (hollow circle) cycles of field sweeping from 240 K to 264 K during heating for $x = 2$ sample. (b) Magnetic entropy change as a function of temperature (ΔS_M versus T) during heating and cooling under the magnetic fields change of 5 T and 7 T estimated using Clausius Clapeyron equation from $M(T)$ curve. The green shaded area is reversible ΔS_M. Comparison of ΔS_M versus T determined from Maxwell relation [Maxwell_$M(\mu_0 H)$], and transformation fraction method [CCTF_$M\mu_0 H$)] during first and second field cycles under (c) 5 T and (d) 7 T, where the second cycle for both cases ΔS_M is reversible.

3(d) compares the ΔS_M of the first cycle obtained from both the CCTF_$M(\mu_0 H)$ equation and Maxwell relation, with the second cycle obtained from the CCTF_$M(\mu_0 H)$ equation under $\mu_0 \Delta H = 5\,T$ and 7 T, respectively (details are shown in Fig. S4 of the Supplemental Material) [36]. In comparison, the ΔS_M value obtained from various methods for the first cycle exhibits good consistency, confirming the validity of the results we obtained. However, it is interesting to note that ΔS_M from the second cycle is almost reversible and reproducible with the first cycle, only with a reduction of $\sim$6% (19.2 J kg^{-1} K^{-1}) and $\sim$4% (22.8 J kg^{-1} K^{-1}) due to $\mu_0 \Delta H$ = 5 T and 7 T, respectively. The obtained maximum reversible ΔS_M value is higher than the largest value reported so far in the all-d-metal Ni(Co)-Mn-Ti Heusler alloys [32,35].

Moreover, operating a magnetic refrigerator under a cyclic low magnetic field change of 1 or 2 T is highly desirable. We have performed $M(T)$ measurements for the field change of 0.05 T, 1 T, 2 T, and 3 T using the isofield measurement protocol shown in Fig. S5 of the Supplemental Material [36]. The application of a 2 T magnetic field shifts the A_S by $\sim$9 K which is comparable to the ΔT_{hys}, exhibiting a partially reversible field-induced IMT. The overlapping area of both the heating and cooling branch produces a large reversible ΔS_M about 9 J kg^{-1} K^{-1} at 269 K which is shown by the blue shaded area in Fig. S5(b) of the Supplemental Material [36]. This magnitude is slightly lower than Ni-Mn-based Heusler alloys but higher than the benchmark material Gd [13].

Another main quantity for a magnetic refrigerant material is the adiabatic temperature change (ΔT_{ad}). We have roughly determined ΔT_{ad} using temperature-dependent specific heat capacity (C_p) from modulated DSC measurement following the equation

$$\Delta T_{ad} = -\frac{T}{C_p} \times \Delta S_M. \tag{8}$$

C_p versus temperature has been measured in zero field conditions using modulated DSC technique as exhibited in Fig. 4(a). Putting reversible ΔS_M obtained from Fig. 3(c) in the above equation, the reversible ΔT_{ad} is obtained and is illustrated as a function of temperature across the IMT in Fig. 4(b). A maximum reversible ΔT_{ad} of $x = 2$ sample $\sim$8.7 K is obtained for the field change of 5 T in our system. The negative ΔT_{ad} corresponding to inverse MCE and the magnitude of reversible ΔT_{ad} at a temperature of 259 K is larger than the reported all-d-metal Heusler alloys [34,35] and similar to the other Ni-Mn-based Heusler systems [6,55,63].

To further investigate the cooling efficiency of the studied system, we have determined the refrigerant capacity (RC), an often useful parameter for practical applications. The RC can be calculated using the formula [64]

$$\mathrm{RC} = \int_{T_{cold}}^{T_{hot}} \Delta S_M dT, \tag{9}$$

where cold end temperatures (T_{cold}) and hot end temperatures (T_{hot}) correspond to the temperature at full width at half maximum of ΔS_M peak. The detailed explanations are given in Sec. S5 of supplemental Material [36]. The obtained giant effective refrigerant capacity (RC_{eff}) of the present $x = 2$ sample is $\sim$382 and 610 J kg^{-1}, respectively, for a magnetic

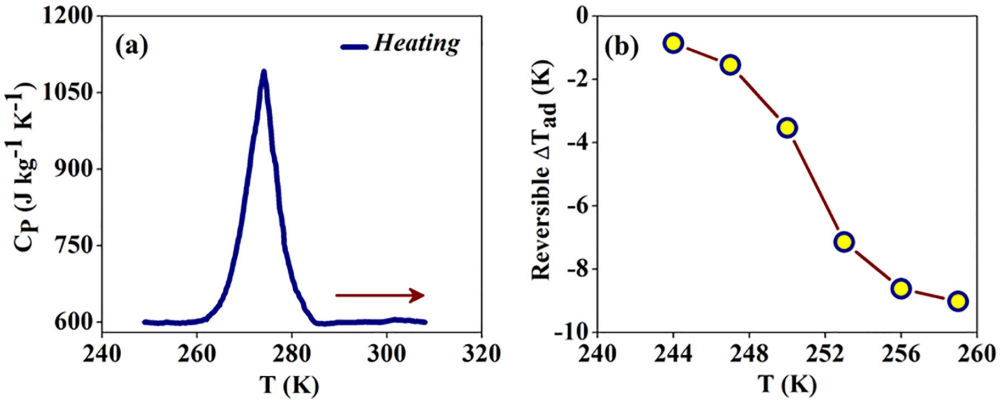

FIG. 4. Temperature-dependent specific heat capacity taken under zero field for heating protocol and (b) reversible ΔT_{ad} as a function of the temperature of $x = 2$ sample.

field change of 5 T and 7 T. Due to the repeatable hysteresis cycle of the $M(\mu_0 H)$ curve of the first-order material, RC_{eff} is taken as a reproducible parameter upon repetitive magnetic field cycling. Therefore, a giant reversible RC_{eff} obtained in our system is the largest value reported so far in all-d-metal Heusler systems and other reported systems [32,34,35,55].

Table II summarizes the magnitude of reversible ΔS_M with the obtained ΔS_M at the first magnetic field cycle at their respective temperatures and corresponding RC reported for different systems with the present system. However, the reversible MCE in each family is significantly limited compared to the first cycle of MCE since Δf_{IA} is not fully achieved. However, the concomitant magnitude of giant reversible and reproducible MCE over a wide temperature range as well as a large RC has been achieved in our system. In view of the solid-state cooling applications, developing an appropriate material with large MCE under a cyclic low magnetic field change of 1 or 2 T with strong mechanical stability is of great importance. Therefore, Cu-doped all-d-metal material is expected to be a conventional MCE material for practical applications.

An irreversible MST can give rise to magnetoplasticity, which manifests as the one-way shape memory effect. Conversely, a complete recovery of the martensite phase may drive the magnetoelasticity, which implies a two-way shape memory effect [65]. Henceforth, the reversibility of the structural transformation relies on the crystalline symmetry and geometric compatibility between the parent and product phase based on the geometrical nonlinear theory of martensite [23,66,67]. Therefore, we determined the geometrical compatibility of the austenite and martensite phase of $x = 2$ sample. We performed temperature-dependent-XRD measurement of the $x = 2$ sample and detailed explanations are given in Sec. S2 of the Supplemental Material [36]. The result shows that the sample undergoes an IMT upon heating from the martensitic phase with a modulated (3M) monoclinic structure ($P2/m$) and a little amount of nonmodulated tetragonal structure ($I4/mmm$) to an austenite B2 cubic structure ($Pm\bar{3}M$). As has been well reported in the literature, the deformation gradient governs the tetragonal structure skeleton into a monoclinic structure [46,68]. The refined lattice parameters at 275 K are $a_c = 5.918$ Å, $a_M = 4.215$ Å, $b_M = 5.501$ Å, $c_M = 12.868$ Å, and

TABLE II. Comparison of reversible magnetic entropy change (ΔS_M) at their respective transition temperatures (T^{peak}), ΔS_M of the first cycle and estimated refrigerant capacity (RC) at the applied field of the present $Ni_{35}Co_{13}Mn_{34.5-x}Cu_xTi_{15.5}$ all-d-metal Heusler system with other related promising systems.

Materials	$\lvert\Delta S_M^{peak}\rvert^{2nd}$ (J kg^{-1} K^{-1})	T^{peak} (K)	$\lvert\Delta S_M^{peak}\rvert^{1st}$ (J kg^{-1} K^{-1})	Applied field (T)	RC (J kg^{-1})	References
Gd	10.2	294		5	462	[13]
$Gd_5(Si_2Ge_2)$	18.5	278		5	462	[12]
$LaFe_{11.4}Si_{1.6}$	19.4	208	19.4	5	427	[52]
$Ni_{49}Co_3Mn_{34}In_{14}$	16.5	268	17.6	3	127	[6]
$Ni_{46}Co_3Mn_{35}Cu_2In_{14}$	16.4	258	16.6	5	490	[39]
$Ni_{50.7}V_{0.3}Mn_{33.4}In_{15.6}$	18.9	276	21	5	252	[53]
$Ni_{41}Ti_1Co_9Mn_{39}Sn_{10}$	18.7	287	21.3	5	540	[48]
$Mn_{0.9}Fe_{0.2}Ni_{0.9}Ge$	18.6	222	39.6	5	252	[54]
$Ni_{49.8}Co_{1.2}Mn_{33.5}In_{15.5}$	14.6	235	15	5	125	[55]
$Ni_{36.5}Co_{13.5}Mn_{35}Ti_{15}B_{0.4}$	18.9	283	24.3	5	278	[35]
$Ni_{36}Co_{14}Mn_{34.5}Ti_{15.5}$	17.8	277	19.8	5	229	[32]
$Ni_{35}Co_{15}Mn_{34.5}Ti_{15.5}$	16.7	243	18.6	5	230	[32]
$Ni_{35}Co_{15}Mn_{34.5-x}Cu_xTi_{15.5}$ $x = 2$	19.2	259	20.2	5	474	Present paper

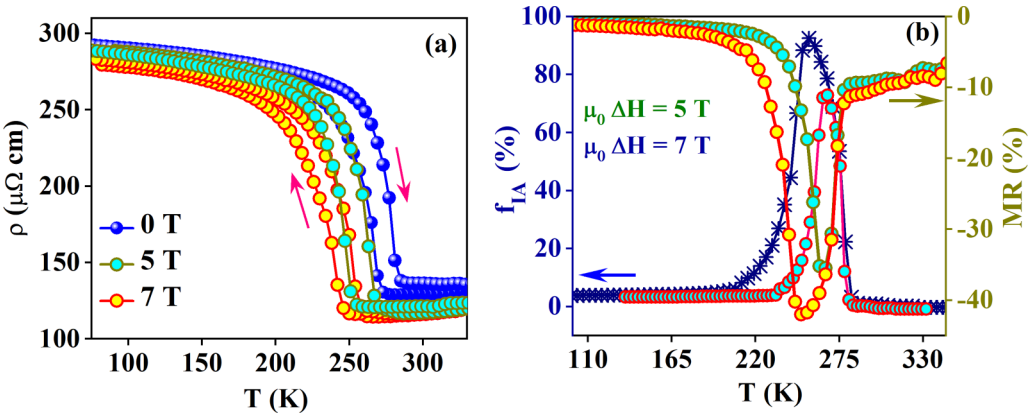

FIG. 5. (a) Temperature dependence of electrical resistivity under 0 T, 5 T, and 7 T for $x = 2$ sample. (b) Austenite phase volume fraction $f_{IA}(T)$ and MR as a function of temperature for the $x = 2$ sample.

$\beta_M = 91.32°$, and $a_t = 4.213$ Å, $c_t = 7.121$ Å for austenite phase and martensitic phase, respectively. By solving the transformation matrix U for cubic to monoclinic transformation, the middle eigenvalue λ_2 is calculated to be 1.0069, closing to unity. Hence, $|1 - \lambda_2| = 0.0069$ with a deviation of 0.69% from the unity indicates that good geometric compatibility for the $x = 2$ sample.

D. Reversible magnetoresistance

The temperature dependence of electrical resistivity on heating and cooling is measured between 50 K to 350 K under 0 T, 5 T, and 7 T magnetic fields as elucidated in Fig. 5(a). The sample is first slowly cooled to 50 K under 0 T, then back to desired temperature under the magnetic field, and $\rho(T)$ data are collected. All $\rho(T)$ curves display an obvious change in resistivity from AFM-like martensite to FM austenite phase across the MST, as evident from the $M(T)$ curve of Fig. 1(b). It is interesting to note that the $\rho(T)$ in the martensitic phase is about 2.2 times larger than that in the austenite phase. This change is attributed to the larger change in the electronic density of states at the Fermi energy, owing to the lattice distortion of the phase transformation [33]. An applied magnetic field of 5 T and 7 T governs in a decrease of T_M and T_A by 17 K, 28 K and 16 K, 26 K with the reduction rate of 3.5, 4, and 3.2, 3.7 K/T, respectively, which is nearly consistent with the $M(T)$ curve. In addition to this shift, a complete reversible IMT and corresponding MR can be expected in the temperature range between 245.7 K (A_f) at 7 T and 254.8 K (M_f) at 0 T where the condition $A_f < M_f$. Note that a partial reversible field-induced IMT would be expected to occur in a wide temperature range between 239.6 K (A_S) at 7 T and 268.8 K (M_S) at 0 T for the $x = 2$ sample.

Figure 5(b) manifests the temperature dependence of MR and $f_{IA}(T, \Delta H)$ under a magnetic field change of $\mu_0 H$ during heating obtained from the following equation:

$$MR = \left[\frac{\rho(\mu_0 H) - \rho(0)}{\rho(0)}\right] \times 100\%, \tag{10}$$

where $\rho(\mu_0 H)$ and $\rho(0)$ stand for the electrical resistance under $\mu_0 H$ and zero field. A maximum MR value of -37.1% and -42.7% are observed across the IMT under the fields of 5 T and 7 T.

Generally, the MR of the metamagnetic Heusler alloy across the IMT can be written as [69]

$$\text{MR} \propto \frac{d\rho}{d\mu_0 H} = \frac{d\rho}{dT}\frac{dT_A}{d\mu_0 H}. \tag{11}$$

With the change in resistivity ($d\rho/dT$) at IMT and the field-induced transformation temperature shift ($dT_A/(d\mu_0 H)$). Therefore, in the application of the magnetic field, two contributions can play a pivotal role in the phase transformation; one is that the free energy of the FM austenite phase decreases because of the change in magnetic energy ($Md\mu_0 H$). Consequently, a higher fraction of the higher resistive AFM martensitic phase is transformed into the FM austenite phase [70]. Hence, a large field-induced downward shift $dT_A/(d\mu_0 H)$ in IMT is observed. Another is the change in resistivity $d\rho/dT$ in the martensite and austenite phases, respectively, without the IMT. Therefore, these contributions would be responsible for the significantly large MR. However, this is the largest reported value so far among the all-d-metal Heusler family and also larger than the other Ni-Mn-based Heusler alloys [19,31,32,34].

To further investigate this $f_{IA}(T, \Delta H)$ mechanism, we have performed isothermal field-dependent resistivity, $\rho(\mu_0 H)$ measurements. For this, we collected $\rho(\mu_0 H)$ data up to third field cycling taken in the above-mentioned temperature intervals, and hence phase fraction-induced MR is ascribed in Figs. 6(a)–6(c), respectively. As the FM austenite phase is energetically favorable to the applied field, the application of the field is equivalent to the rise of temperature. Consider a coexisting region with martensitic and austenite phase fractions as $f_M(T, H)$ and $f_A(T, H) = 1 - f_M(T, H)$ [71]. When the field is increased isothermally from 0 T, due to the field-assisted nature of austenite, the energy barrier between the two phases decreases. Progressively, the more martensitic phase transforms into the austenite phase. For example, the phase fraction at 255 K goes from 0.9% to 94% for 7 T while the remaining 6% is unchanged. Once the field is reduced to zero, this smaller residual 6% causes the arrested phase and the rest portion can participate reversibly for the second and subsequent field cyclic measurements. Note that this residual austenite is unchanged until the energy barrier height is altered by changing T or $\mu_0 H$. Therefore, 40% of reversible MR out of 42% is obtained. Furthermore, with the temperature

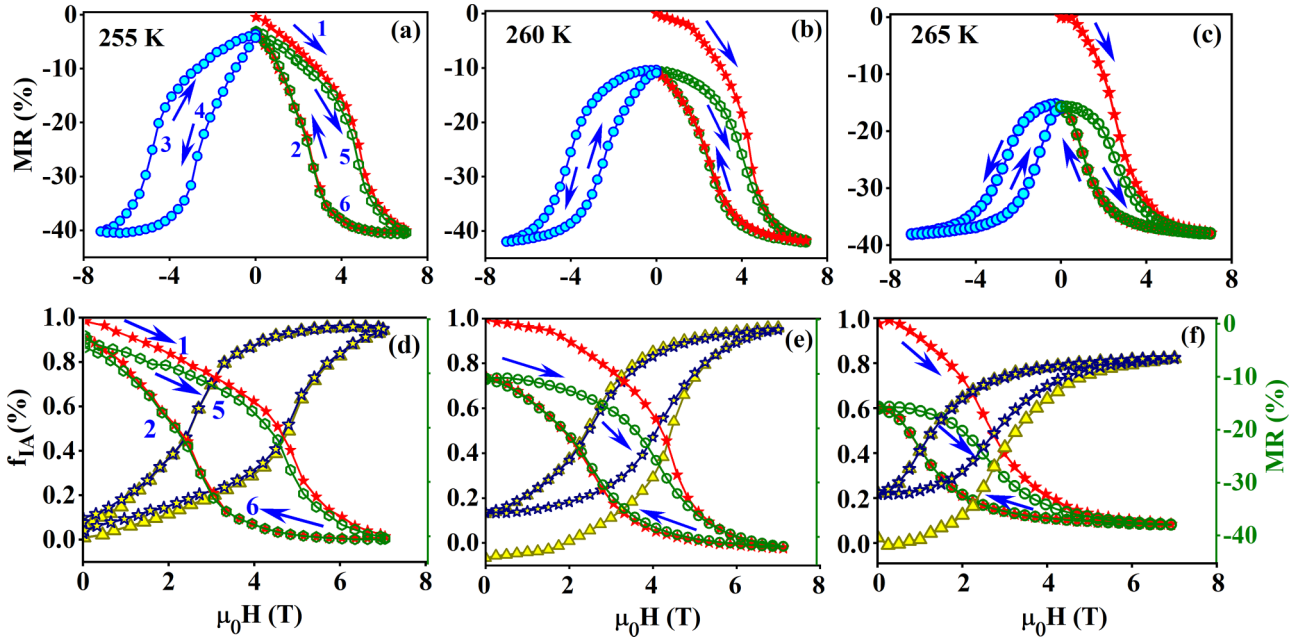

FIG. 6. Field dependence of MR at (a) 255 K, (b) 260 K, and (c) 265 K upon heating mode across the transition for $x = 2$ sample. The solid red star points represent first cycle and the rest are the second and third cycles ρ-H of the magnetic field. (d)–(f) Austenite phase volume fraction $f_{IA}(T)$ and MR for the $x = 2$ sample at their corresponding temperatures.

increment, for example, 260 K and 265 K, further increase of $\mu_0 H$ governs a higher amount of austenite and the region attains different $f_M(T, H)$ and $f_A(T, H)$ ratios through the minimization of the free energy barrier. Consequently, a decrease of reversible MR from 31% to 22% is due to a decrease of $f_{IA}(T, H)$ from 82% to 59% from 260 K to 265 K. Therefore, $f_{IA}(T, H)$ is a decisive factor to tune the reversible MR in this system.

IV. CONCLUSIONS

In summary, a giant reversible MCE and MR have been experimentally obtained by varying the field-induced phase fraction. We demonstrate the evolution of Δf_{IA} using the CCE and the Landauer equation under field cycling, leading to a realization of enhanced reversible magnetoresponsive properties of the optimized $x = 2$ sample. Moreover, the sample exhibited larger MST sensitivity to the field $\sim 4.3\,\mathrm{K}/T$ and low thermal hysteresis ~ 8.3 K, which is evidenced by good crystallographic compatibility. Subsequently, a giant reversible ΔS_M of about 22.8 J kg^{-1} K^{-1} ($\sim 96\%$) over a wide temperature range ~ 20 K (9 J kg^{-1} K^{-1} at 269 K for 2 T) and giant reversible MR of 40% over 42% of the total MR in a field change of 7 T is observed when field-induced IMT is fully induced. The obtained magnitude of reversible ΔS_M and MR is the highest reported value so far in the all-d-metal Heusler family. The concurrent observation of giant ΔS_M, RC_{eff} and MR is also very rare in Heusler alloys. Hence, our results can provide the generality of utilizing the Δf_{IA} to realize the enhanced magnetoresponsive properties in conventional all-d-metal Heusler system. Moreover, the synergistic combinations of giant MCE and MR by proper tailoring of Cu-doped all-d-metal Heusler alloys may lead a diverse range of solid state-based technological applications.

ACKNOWLEDGMENTS

S.S. acknowledges S. N. Bose National Centre for Basic Sciences for the Bridge Fellowship. Financial help from the Department of Science and Technology, Government of India, through Project No. TAR/2019/000284 is sincerely acknowledged.

[1] T. Krenke, E. Duman, M. Acet, E. F. Wassermann, X. Moya, L. Mañosa, and A. Planes, Nat. Mater. **4**, 450 (2005).
[2] R. Kainuma, Y. Imano, W. Ito, H. Morito, Y. Sutou, K. Oikawa, A. Fujita, K. Ishida, S. Okamoto, O. Kitakami *et al.*, Appl. Phys. Lett. **88**, 192513 (2006).
[3] J. Liu, T. Gottschall, K. P. Skokov, J. D. Moore, and O. Gutfleisch, Nat. Mater. **11**, 620 (2012).
[4] M. Khan, I. Dubenko, S. Stadler, and N. Ali, J. Appl. Phys. **102**, 113914 (2007).
[5] L. Chen, F. Hu, J. Wang, L. Bao, J. Sun, B. Shen, J. Yin, and L. Pan, Appl. Phys. Lett. **101**, 012401 (2012).
[6] X. M. Sun, D. Y. Cong, Z. Li, Y. L. Zhang, Z. Chen, Y. Ren, K.-D. Liss, Z. Y. Ma, R. G. Li, Y. H. Qu, Z. Yang, L. Wang, and Y. D. Wang, Phys. Rev. Mater. **3**, 034404 (2019).
[7] Y. Sutou, Y. Imano, N. Koeda, T. Omori, R. Kainuma, K. Ishida, and K. Oikawa, Appl. Phys. Lett. **85**, 4358 (2004).
[8] H. E. Karaca, I. Karaman, B. Basaran, Y. Ren, Y. I. Chumlyakov, and H. J. Maier, Adv. Funct. Mater. **19**, 983 (2009).

[9] M. Chmielus, X. Zhang, C. Witherspoon, D. Dunand, and P. Müllner, Nat. Mater. **8**, 863 (2009).
[10] Z. Liu, M. Zhang, Y. Cui, Y. Zhou, W. Wang, G. Wu, X. Zhang, and G. Xiao, Appl. Phys. Lett. **82**, 424 (2003).
[11] V. K. Pecharsky and K. A. Gschneidner Jr., Adv. Mater. **13**, 683 (2001).
[12] V. K. Pecharsky and K. A. Gschneidner Jr., Phys. Rev. Lett. **78**, 4494 (1997).
[13] S. Y. Dan'kov, A. M. Tishin, V. K. Pecharsky, and K. A. Gschneidner, Phys. Rev. B **57**, 3478 (1998).
[14] V. Franco, J. Blázquez, J. Ipus, J. Law, L. Moreno-Ramírez, and A. Conde, Prog. Mater. Sci. **93**, 112 (2018).
[15] J.-H. Chen, A. Us Saleheen, S. K. Karna, D. P. Young, I. Dubenko, N. Ali, and S. Stadler, J. Appl. Phys. **124**, 203903 (2018).
[16] E. Liu, W. Wang, L. Feng, W. Zhu, G. Li, J. Chen, H. Zhang, G. Wu, C. Jiang, H. Xu *et al.*, Nat. Commun. **3**, 873 (2012).
[17] J. S. Mohanty, S. Samanta, and K. Mandal, J. Magn. Magn. Mater. **578**, 170834 (2023).
[18] X. Moya, L. Mañosa, A. Planes, S. Aksoy, M. Acet, E. F. Wassermann, and T. Krenke, Phys. Rev. B **75**, 184412 (2007).
[19] Z. Wei, E. Liu, J. Chen, Y. Li, G. Liu, H. Luo, X. Xi, H. Zhang, W. Wang, and G. Wu, Appl. Phys. Lett. **107**, 022406 (2015).
[20] V. G. de Paula and M. S. Reis, Chem. Mater. **33**, 5483 (2021).
[21] E. Şaşıoğlu, L. M. Sandratskii, and P. Bruno, Phys. Rev. B **77**, 064417 (2008).
[22] R. Zarnetta, R. Takahashi, M. L. Young, A. Savan, Y. Furuya, S. Thienhaus, B. Maaß, M. Rahim, J. Frenzel, H. Brunken *et al.*, Adv. Funct. Mater. **20**, 1917 (2010).
[23] Y. Song, X. Chen, V. Dabade, T. W. Shield, and R. D. James, Nature **502**, 85 (2013).
[24] H. Qian, J. Guo, Z. Wei, and J. Liu, Phys. Rev. Mater. **6**, 054401 (2022).
[25] F. Zhang, K. Westra, Q. Shen, I. Batashev, A. Kiecana, N. van Dijk, and E. Brück, J. Alloys Compd. **906**, 164337 (2022).
[26] H. N. Bez, A. K. Pathak, A. Biswas, N. Zarkevich, V. Balema, Y. Mudryk, D. D. Johnson, and V. K. Pecharsky, Acta Mater. **173**, 225 (2019).
[27] A. Taubel, B. Beckmann, L. Pfeuffer, N. Fortunato, F. Scheibel, S. Ener, T. Gottschall, K. P. Skokov, H. Zhang, and O. Gutfleisch, Acta Mater. **201**, 425 (2020).
[28] S. Samanta, S. Ghosh, and K. Mandal, J. Phys.: Condens. Matter **34**, 105801 (2022).
[29] D. Cong, W. Xiong, A. Planes, Y. Ren, L. Mañosa, P. Cao, Z. Nie, X. Sun, Z. Yang, X. Hong *et al.*, Phys. Rev. Lett. **122**, 255703 (2019).
[30] A. Aznar, A. Gràcia-Condal, A. Planes, P. Lloveras, M. Barrio, J.-L. Tamarit, W. Xiong, D. Cong, C. Popescu, and L. Mañosa, Phys. Rev. Mater. **3**, 044406 (2019).
[31] K. Liu, S. Ma, C. Ma, X. Han, K. Yu, S. Yang, Z. Zhang, Y. Song, X. Luo, C. Chen *et al.*, J. Alloys Compd. **790**, 78 (2019).
[32] S. Samanta, S. Chatterjee, S. Ghosh, and K. Mandal, Phys. Rev. Mater. **6**, 094411 (2022).
[33] Q. Zeng, J. Shen, H. Zhang, J. Chen, B. Ding, X. Xi, E. Liu, W. Wang, and G. Wu, J. Phys.: Condens. Matter **31**, 425401 (2019).
[34] S. Samanta, S. Ghosh, S. Chatterjee, and K. Mandal, J. Alloys Compd. **910**, 164929 (2022).
[35] F. Zhang, I. Batashev, N. van Dijk, and E. Bruck, Phys. Rev. Appl. **17**, 054032 (2022).
[36] See Supplemental Material at http://link.aps.org/supplemental/10.1103/PhysRevMaterials.7.084406 for sample characterizations, geometrical compatibility analysis, calometric study, and additional magnetic analysis, which also includes Ref. [72].
[37] P. Devi, C. S. Mejía, L. Caron, S. Singh, M. Nicklas, and C. Felser, Phys. Rev. Mater. **3**, 122401(R) (2019).
[38] S. Roy, E. Blackburn, S. M. Valvidares, M. R. Fitzsimmons, S. C. Vogel, M. Khan, I. Dubenko, S. Stadler, N. Ali, S. K. Sinha, and J. B. Kortright, Phys. Rev. B **79**, 235127 (2009).
[39] Z. Li, J. Yang, D. Li, Z. Li, B. Yang, H. Yan, C. F. Sánchez-Valdés, J. L. S. Llamazares, Y. Zhang, C. Esling *et al.*, Adv. Electron. Mater. **5**, 1800845 (2019).
[40] A. T. Zayak, P. Entel, K. M. Rabe, W. A. Adeagbo, and M. Acet, Phys. Rev. B **72**, 054113 (2005).
[41] F. Cugini, S. Chicco, F. Orlandi, G. Allodi, P. Bonfá, V. Vezzoni, O. N. Miroshkina, M. E. Gruner, L. Righi, S. Fabbrici *et al.*, Phys. Rev. B **105**, 174434 (2022).
[42] C. Salazar Mejía, M. Ghorbani Zavareh, A. Nayak, Y. Skourski, J. Wosnitza, C. Felser, and M. Nicklas, J. Appl. Phys. **117**, 17E710 (2015).
[43] E. Cesari, D. Salas, and S. Kustov, Mater. Sci. Forum. **684**, 49 (2011).
[44] T. Kihara, X. Xu, W. Ito, R. Kainuma, and M. Tokunaga, Phys. Rev. B **90**, 214409 (2014).
[45] T. Gottschall, K. P. Skokov, D. Benke, M. E. Gruner, and O. Gutfleisch, Phys. Rev. B **93**, 184431 (2016).
[46] L. Silva, J. Patiño, and A. Gomes, J. Phys.: Condens. Matter **33**, 235701 (2021).
[47] V. Khovaylo, J. Alloys Compd. **577**, S362 (2013).
[48] Y. Qu, D. Cong, X. Sun, Z. Nie, W. Gui, R. Li, Y. Ren, and Y. Wang, Acta Mater. **134**, 236 (2017).
[49] L. Caron, Z. Ou, T. Nguyen, D. C. Thanh, O. Tegus, and E. Brück, J. Magn. Magn. Mater. **321**, 3559 (2009).
[50] K. Xu, Z. Li, Y.-L. Zhang, and C. Jing, Phys. Lett. A **379**, 3149 (2015).
[51] R. Landauer, J. Appl. Phys. **23**, 779 (1952).
[52] F.-x. Hu, B.-g. Shen, J.-r. Sun, Z.-h. Cheng, G.-h. Rao, and X.-x. Zhang, Appl. Phys. Lett. **78**, 3675 (2001).
[53] J. Liu, X. You, B. Huang, I. Batashev, M. Maschek, Y. Gong, X. Miao, F. Xu, N. van Dijk, and E. Brück, Phys. Rev. Mater. **3**, 084409 (2019).
[54] J. Liu, Y. Gong, Y. You, X. You, B. Huang, X. Miao, G. Xu, F. Xu, and E. Brück, Acta Mater. **174**, 450 (2019).
[55] L. Huang, D. Cong, L. Ma, Z. Nie, Z. Wang, H. Suo, Y. Ren, and Y. Wang, Appl. Phys. Lett. **108**, 032405 (2016).
[56] M. Modak, M. K. Ray, S. Mondal, B. Maji, K. Bagani, A. Bhattacharyya, and S. Banerjee, J. Phys. D **53**, 205301 (2020).
[57] S. Yu, L. Ma, G. Liu, Z. Liu, J. Chen, Z. Cao, G. Wu, B. Zhang, and X. Zhang, Appl. Phys. Lett. **90**, 242501 (2007).
[58] L. Caron, N. B. Doan, and L. Ranno, J. Phys.: Condens. Matter **29**, 075401 (2017).
[59] A. Ghosh, R. Rawat, A. Bhattacharyya, G. Mandal, A. Nigam, and S. Nair, J. Magn. Magn. Mater. **476**, 92 (2019).
[60] K. Dubey, P. Devi, A. K. Singh, and S. Singh, J. Magn. Magn. Mater. **507**, 166818 (2020).

[61] K. A. Gschneidner, V. Pecharsky, and A. Tsokol, Rep. Prog. Phys. **68**, 1479 (2005).
[62] P. J. Shamberger and F. S. Ohuchi, Phys. Rev. B **79**, 144407 (2009).
[63] P. Devi, C. S. Mejía, M. G. Zavareh, K. K. Dubey, P. Kushwaha, Y. Skourski, C. Felser, M. Nicklas, and S. Singh, Phys. Rev. Mater. **3**, 062401(R) (2019).
[64] V. Provenzano, A. J. Shapiro, and R. D. Shull, Nature **429**, 853 (2004).
[65] J. Liu, N. Scheerbaum, J. Lyubina, and O. Gutfleisch, Appl. Phys. Lett. **93**, 102512 (2008).
[66] K. Bhattacharya, S. Conti, G. Zanzotto, and J. Zimmer, Nature **428**, 55 (2004).
[67] J. Cui, Y. S. Chu, O. O. Famodu, Y. Furuya, J. Hattrick-Simpers, R. D. James, A. Ludwig, S. Thienhaus, M. Wuttig, Z. Zhang *et al.*, Nat. Mater. **5**, 286 (2006).
[68] R. D. James and K. F. Hane, Acta Mater. **48**, 197 (2000).
[69] J. M. Barandiarán, V. A. Chernenko, P. Lázpita, J. Gutiérrez, and J. Feuchtwanger, Phys. Rev. B **80**, 104404 (2009).
[70] T. Samanta, A. Us Saleheen, D. L. Lepkowski, A. Shankar, I. Dubenko, A. Quetz, M. Khan, N. Ali, and S. Stadler, Phys. Rev. B **90**, 064412 (2014).
[71] S. Chatterjee, S. Giri, S. Majumdar, and S. K. De, Phys. Rev. B **77**, 224440 (2008).
[72] Y. Qu, D. Cong, S. Li, W. Gui, Z. Nie, M. Zhang, Y. Ren, and Y. Wang, Acta Mater. **151**, 41 (2018).